Inorganic Chemistry

Article

pubs.acs.org/IC

Strong Energy-Transfer-Induced Enhancement of Luminescence Efficiency of Eu^{2+}- and Mn^{2+}-Codoped Gamma-AlON for Near-UV-LED-Pumped Solid State Lighting

Lihong Liu,[†,‡] Le Wang,*[,†] Chenning Zhang,[§] Yujin Cho,[∥,⊥] Benjamin Dierre,[∥] Naoto Hirosaki,[‡] Takashi Sekiguchi,[∥,⊥] and Rong-Jun Xie*[,‡]

[†]College of Optics and Electronic Science and Technology, China Jiliang University, Hangzhou 310018, China

[‡]Sialon Group, Sialon Unit and [∥]Nano Device Characterization Group, MANA, National Institute for Materials Science, Namiki 1-1, Tsukuba, Ibaraki 305-0044, Japan

[§]Fine Particles Engineering Group, Materials Processing Unit, National Institute for Materials Science, Tsukuba, Ibaraki 305-0047, Japan

[⊥]Graguate School of Pure and Applied Science, University of Tsukuba, Tsukuba, Ibaraki 305-0003, Japan

ABSTRACT: A series of Eu^{2+}- and Mn^{2+}-codoped γ-AlON ($Al_{1.7}O_{2.1}N_{0.3}$) phosphors was synthesized at 1800 °C under 0.5 MPa N_2 by using the gas-pressure sintering method (GPS). Eu^{2+} and Mn^{2+} ions were proved to enter into γ-AlON host lattice by means of XRD, CL, and EDS measurements. Under 365 nm excitation, two emission peaks located at 472 and 517 nm, resulting from $4f^6 5d^1 \rightarrow 4f^7$ and $^4T_1(4G) \rightarrow {}^6A_1$ electron transitions of Eu^{2+} and Mn^{2+}, respectively, can be observed. Energy transfer from Eu^{2+} to Mn^{2+} was evidenced by directly observing appreciable overlap between the excitation spectrum of Mn^{2+} and the emission spectrum of Eu^{2+} as well as by the decreased decay time of Eu^{2+} with increasing Mn^{2+} concentration. The critical energy-transfer distance between Eu^{2+} and Mn^{2+} and the energy-transfer efficiency were also calculated. The mechanism of energy transfer was identified as a resonant type via a dipole−dipole mechanism. The external quantum efficiency was increased 7 times (from 7% for γ-AlON:Mn^{2+} to 49% for γ-AlON:Mn^{2+},Eu^{2+} under 365 nm excitation), and color-tunable emissions from blue-green to green-yellow were also realized with the $Eu^{2+} \rightarrow Mn^{2+}$ energy transfer in γ-AlON.

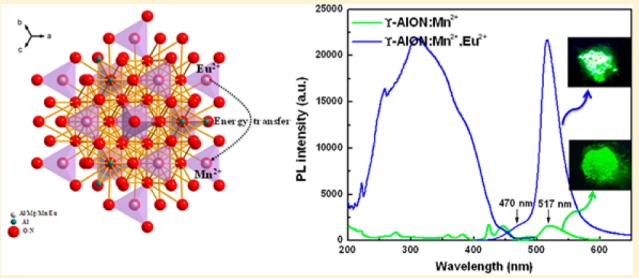

I. INTRODUCTION

Phosphor-converted white light-emitting diodes (wLEDs) are high-quality, high-efficiency solid state lighting sources that promise to strengthen our energy security, reduce the carbon emissions, and revitalize our economy.[1,2] As one of the key materials, phosphors play a crucial role in determining the optical quality, lifetime, and cost of wLEDs.[3] Accordingly, both development of novel phosphors and improvement of the existing ones are of great importance to produce highly efficient and reliable lighting devices and to contribute to the development of materials science and technology. Among a large number of phosphor materials, rare-earth-doped nitride and oxynitride phosphors, such as $M[LiAl_3N_4]:Eu^{2+}$ (M = Ca, Sr), $Ba_5Si_{11}Al_7N_{25}:Eu^{2+}$, $BaSi_4Al_7N_9:Eu^{2+}$, $M[Mg_3SiN_4]:Ce^{3+}$ (M = Ca, Sr, Eu), $Ca_{15}Si_{20}N_{30}O_{10}:Eu^{2+}$, β-sialon:Eu^{2+}, α-sialon:Eu^{2+}, $(Ca,Sr,Ba)_2Si_5N_8:Eu^{2+}$, $CaSiAlN_3:Ce^{3+}$, and $CaSiAlN_3:Eu^{2+}$ have attracted much attention, due to their strong absorption of the UV-to-blue light, significantly red-shifted luminescence spectra, high emission efficiency, and small thermal quenching.[1−11] These excellent photoluminescence properties enable them to be used in phosphor-converted white LEDs to achieve high color rendition or high luminous efficiency.

γ-AlON, a solid−solution compound in the binary system of AlN−Al_2O_3, is well known for its use as a transparent ceramic material owing to its high thermomechanical properties and large band gap.[12] When doped with Mn^{2+} or rare earths, γ-AlON can also be developed into interesting luminescent materials.[12−15] γ-AlON:Mn^{2+} is a promising green phosphor for wLEDs, exhibiting a narrow emission band centered at 520 nm, a small thermal quenching, and high internal quantum efficiency of 62% under blue light irradiation.[15] By carrying out the synchrotron X-ray diffraction and absorption fine structure measurements, Takeda confirmed the divalent state of manganese in γ-AlON that occupied the tetrahedral sites.[16] On the other hand, γ-AlON:Mn^{2+} has a quite low absorption efficiency (16% and 21% under 365 and 450 nm excitation, respectively) due to the spin-forbidden transition of $3d^5$ electrons in Mn^{2+}, so that it is hardly used in wLEDs.

One of the strategies for overcoming the low absorption of Mn^{2+} is to codope a sensitizer that would transfer its energy to Mn^{2+}. Eu^{2+} has been reported to be an efficient sensitizer for Mn^{2+} in a number of oxidic phosphors.[17−26] For example,

Received: March 26, 2015
Published: May 20, 2015

DOI: 10.1021/acs.inorgchem.5b00683
Inorg. Chem. 2015, 54, 5556−5565

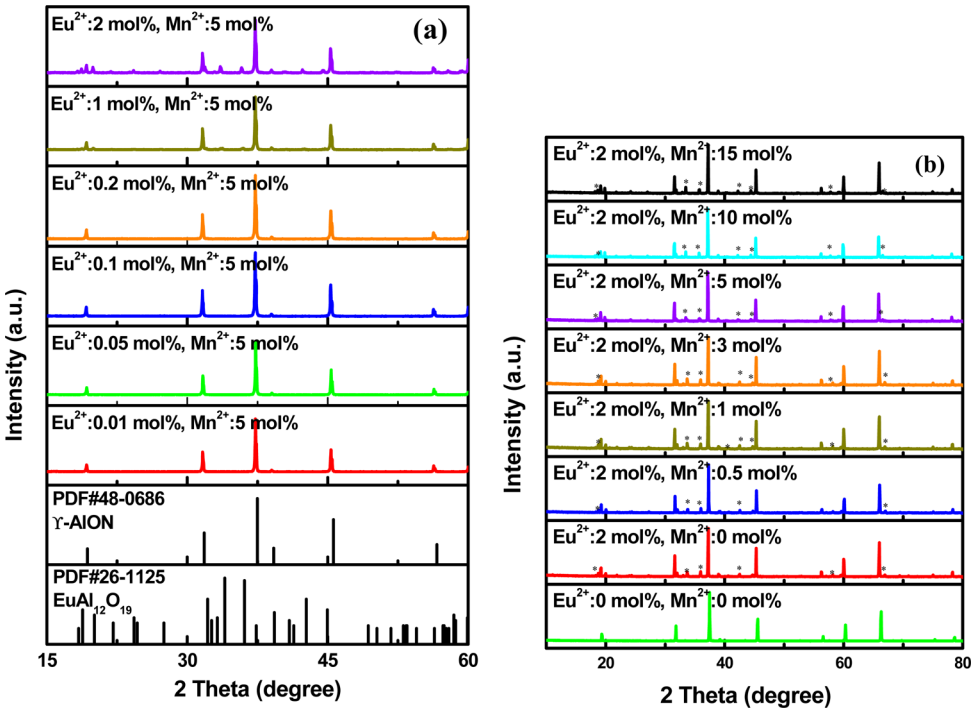

Figure 1. XRD patterns of (a) γ-AlON:5 mol % Mn^{2+} doped with varying Eu^{2+} concentrations and (b) γ-AlON:2 mol % Eu^{2+} doped with varying Mn^{2+} concentrations.

Kwon evidenced the enhanced red emission of Mn^{2+} in $Ca_{6-x-y}Mg_{x\ z}(PO_4)_4$:$Mn^{2+}$,$Eu^{2+}$ through the energy transfer from Eu^{2+} to Mn^{2+}. Although there have been no reports on such an energy transfer in nitridic phosphors to the best of our knowledge, it is anticipated that the energy-transfer strategy can also make sense if both Mn^{2+} and Eu^{2+} concentrations are carefully controlled.

Therefore, in this work we prepared the Eu^{2+}- and Mn^{2+}-codoped γ-AlON phosphors by the gas-pressure sintering approach and investigated their photoluminescence spectra, cathodoluminescence (CL), quantum efficiency, absorption, thermal quenching, and decay times. The energy transfer between Eu^{2+} and Mn^{2+} and its mechanism were discussed. The experimental results showed that the energy transfer definitely occurred in γ-AlON:Mn^{2+},Eu^{2+} and led to significant increases in both luminescence and quantum efficiency. These improvements together with the good thermal stability enable the title phosphor to be used as a green luminescent material in UV-LED pumped wLEDs.

II. EXPERIMENTAL SECTION

A series of γ-ALON:$x$$Mn^{2+}$,$y$$Eu^{2+}$ ($Al_{1.7}O_{2.1}N_{0.3}$, x = 0−15 mol %, y = 0.01−2 mol %) phosphors was prepared by firing the powder mixtures of AlN (Tokuyama, E-grade), Al_2O_3 (Taimei Chemical, 4N), MgO (Kojyundo Chemical, 3N), Eu_2O_3 (Shin-Etsu Chemical Co. Ltd.), and $MnCO_3$ (Shin-Etsu Chemical Co. Ltd.) in a gas-pressure furnace (FVPHR-R-10, FRET-40, Fujidempa Kogyo Co. Ltd., Osaka, Japan) with a graphite heater. For each composition, a total of 2 g was weighed out from the starting powders and well mixed in a mortar by hand. The powder mixtures were packed into boron nitride crucibles with a diameter of 20 mm and heated with a constant heating rate of 600 °C/h in vacuum (<10^{-3} Pa) from room temperature to 800 °C. At 800 °C, nitrogen gas (99.999% purity) was introduced into the chamber. The powder samples were heated at 1800 °C for 2 h under a nitrogen gas pressure of 1.0 MPa. After firing, the electric power was shut off, and the samples were cooled down naturally with the furnace.

The phase identification of the synthesized powders was performed by X-ray powder diffraction (XRD, Smart Lab, Rigaku) operating at 40 kV and 40 mA and using Cu Kα_1 radiation (λ = 1.5406 Å). A step size of 0.02° was used with a scan speed of 2°/min.

SEM and CL measurements were executed by a field emission SEM (Hitachi, S4300) equipped with a CL system (Horiba, MP32S/M). Energy-dispersed X-ray spectroscopy (EDS) measurements were carried out at room temperature using a high-resolution field emission scanning electron microscope (Hitachi, S4800).

Diffuse reflection spectra were recorded in a Hamamatsu MPCD-7000 multichannel photodetector. Photoluminescence spectra were measured at room temperature using a fluorescent spectrophotometer (F-4500, Hitachi Ltd., Tokyo, Japan) with a 200 W Xe lamp as an excitation source. The emission spectrum was corrected for the spectral response of a monochromator and Hamamatsu R928P photomultiplier tube by a light diffuser and a tungsten lamp (Noma, 10 V, 4 A). The excitation spectrum was also corrected for the spectral distribution of xenon lamp intensity by measuring rhodamine B as reference.

Time-resolved PL measurements were conducted using a time-correlated single-photon counting fluorometer (TemPro, Horiba Jobin-Yvon) equipped with LED excitation sources of 455 and 493 nm with a pulse duration full width at half-maximum of ∼1 ns. Thermal quenching was evaluated by measuring the temperature-dependent photoluminescence in the Hamamatsu MPCD-7000 multichannel photodetector with a 200 W Xe-lamp as an excitation source. The phosphor powder was loaded in a hot plate connected to MPCD-7000 and then heated to the desired temperature with a heating rate of 100 °C/min. The sample was held at a certain temperature for 5 min to reach thermal equilibrium, which will guarantee a uniform temperature distribution both in the surface and in the interior of the samples.

III. RESULTS AND DISCUSSION

Phase Identification. Figure 1a presents XRD patterns of γ-AlON:5 mol % Mn^{2+},$y$$Eu^{2+}$ doped with varying Eu^{2+} concentrations (y = 0−2 mol %). A phase-pure cubic γ-AlON (PDF No. 48-0686) is detected when the concentration of Eu^{2+}

DOI: 10.1021/acs.inorgchem.5b00683
Inorg. Chem. 2015, 54, 5556−5565

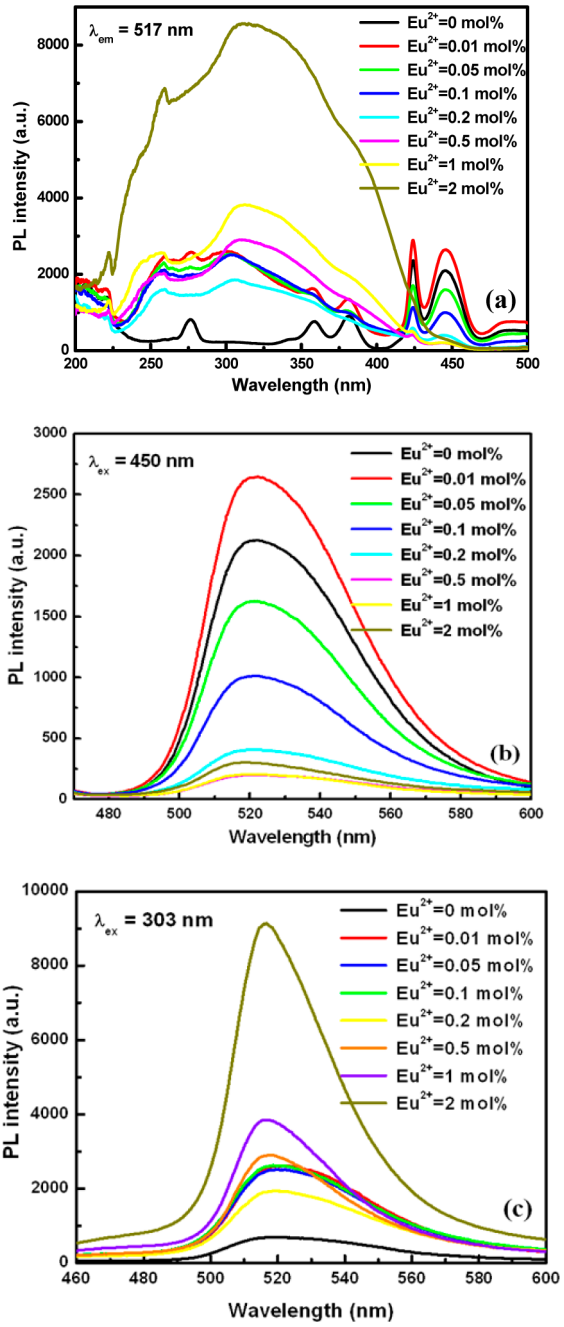

Figure 2. (a) Excitation spectra monitored at 517 nm and emission spectra measured under 450 (b) and 303 nm (c) excitation of γ-AlON:5 mol % Mn^{2+}, yEu^{2+} with varying Eu^{2+} concentrations (y = 0–2 mol %).

is smaller than 0.2 mol %. A minor impurity phase of $EuAl_{12}O_{19}$ (PDF No. 26-1125) also appears in samples with higher Eu^{2+} concentrations, indicating that the solubility of Eu^{2+} in γ-AlON is very limited due to the large difference in ionic size of Al^{3+} (0.39 Å, 4CN) and Eu^{2+} (1.17 Å, 4CN).[27] At y = 2 mol %, the weight percentage of the impurity phase is about 40%. As seen in Figure 1b, the amount of $EuAl_{12}O_{19}$ remains unchanged in samples with varying Mn^{2+} concentrations and a fixed Eu^{2+} content (2 mol %). To know the exact amount of Eu^{2+} accommodated in γ-AlON:Eu^{2+},Mn^{2+}, we calculated it by considering the consumption of Eu^{2+} with the formation of $EuAl_{12}O_{19}$. The real concentration of Eu^{2+} is then estimated as

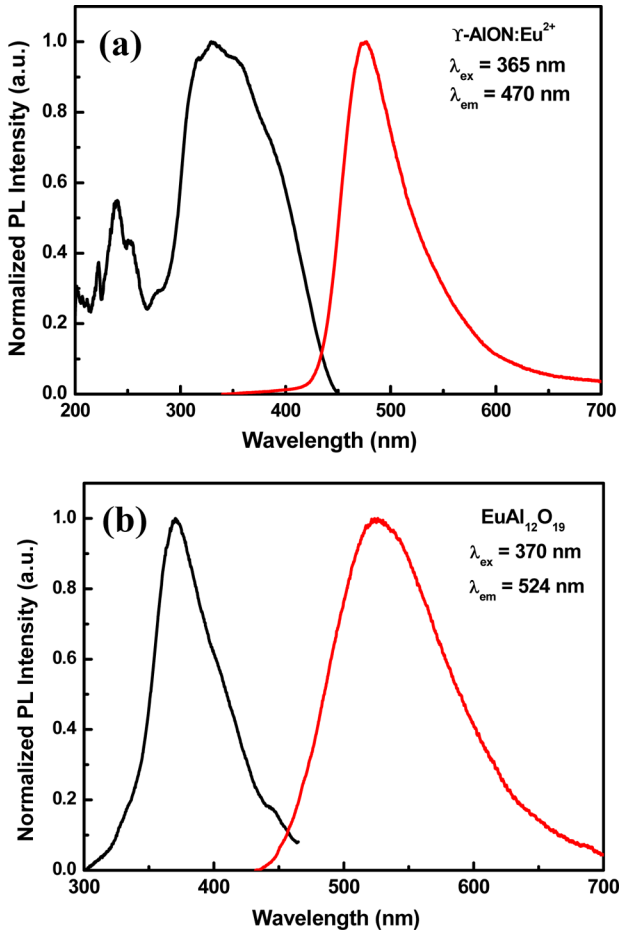

Figure 3. Photoluminescence spectra of (a) γ-AlON:Eu^{2+} and (b) $EuAl_{12}O_{19}$.

1.9 mol % for each sample, which is very close to 2.0 mol % designed for the samples with varying Mn^{2+} concentrations.

Photoluminescence Spectra. We reported that γ-AlON:Mn^{2+} displays a narrow emission band (with a full-width at half-maximum of ~45 nm) centered at 517 nm due to $^4T_1(4G)$–$^6A_1$ transition of Mn^{2+} under 450 nm excitation. Its excitation spectrum consists of several bands centered at 275, 356, 376, 423, and 444 nm corresponding to electronic transitions of Mn^{2+} from $^6A_1$ to $^4T_2$ (^4P), ^4E (^4G), $^4T_2$, [^4E (^4G), ^4A (^4G)], and $^4T_2$ (^4G), respectively. On the other hand, once Eu^{2+} is codoped into γ-AlON, the excitation spectrum changes significantly (Figure 2a), with the characteristic sharp lines of Mn^{2+} turning into a very broad band covering the spectral range of 200–400 nm and the absorption of the UV light being dramatically enhanced. This leads to the decrease of the luminescence intensity under 450 nm excitation (Figure 2b) but the increase of the PL intensity under 303 nm excitation (Figure, 2c) as the Eu^{2+} concentration increases. It implies that the energy transfer between Eu^{2+} and Mn^{2+} occurs and contributes to the great enhancement of the excitation spectrum in the UV region. Furthermore, a shoulder emission at 470 nm is seen in the codoped samples when excited at 303 nm, which is believed to be the emission of Eu^{2+} in γ-AlON rather than the Mn^{2+} emission in the impurity phase $EuAl_{12}O_{19}$ (because the latter has no luminescence at all).

The excitation spectrum of the sample solely doped with Eu^{2+} has a broad band owing to the $4f^7$–$4f^65d^1$ transition of

DOI: 10.1021/acs.inorgchem.5b00683
Inorg. Chem. 2015, 54, 5556–5565

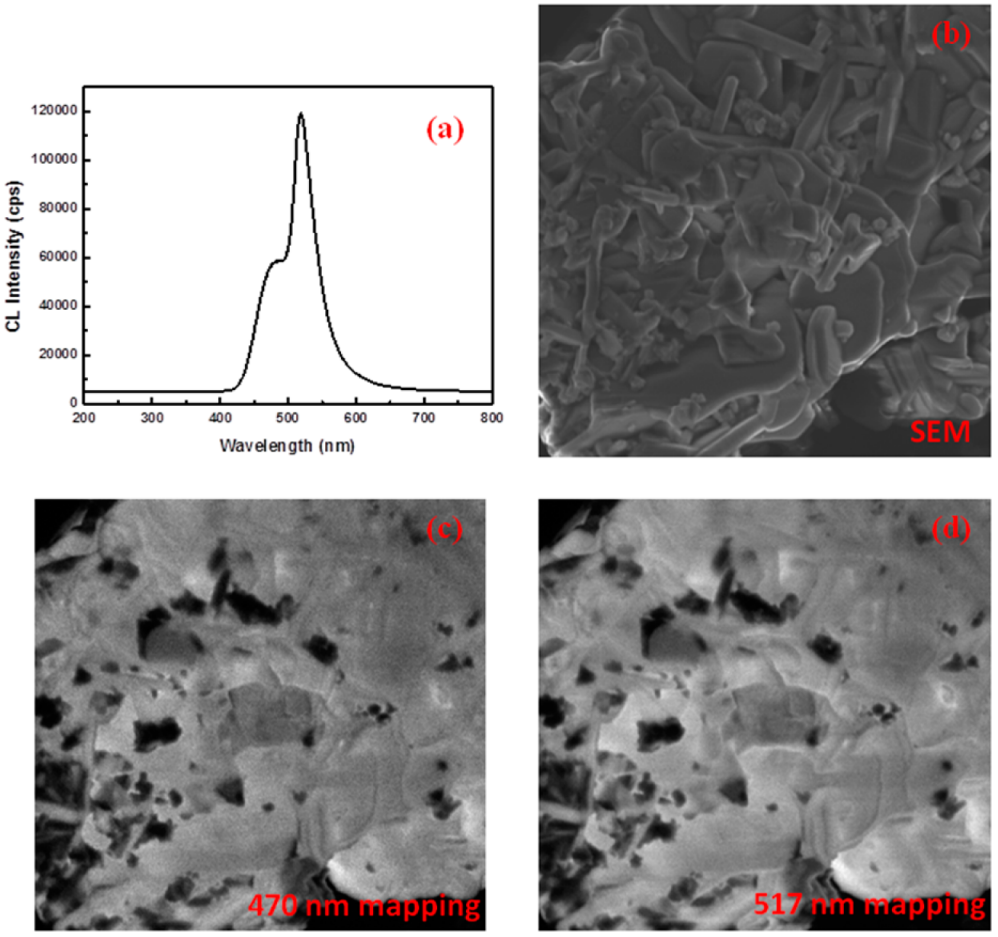

Figure 4. (a) CL spectra and (b) SEM image and CL images taken at wavelengths of 470 (c) and 517 nm (d) for γ-AlON:2 mol % Eu^{2+}, 5 mol % Mn^{2+}.

Eu^{2+} (Figure 3a). Under 365 nm excitation, γ-AlON:Eu^{2+} shows a broad emission band centered at 470 nm, which is in accordance with the previous study repored by Wang et al.[28] In addition, the impurity phase $EuAl_{12}O_{19}$ gives a very weak green emission at about 524 nm (Figure 3b), so that its emission can be omitted in the codoped samples.

For γ-AlON:Eu^{2+},Mn^{2+}, the PL spectrum consists of a broad band centered at 470 nm and an intense narrow band at 517 nm. It is believed that these two emission bands correspond to emissions of γ-AlON:Mn^{2+} and γ-AlON:Eu^{2+}, respectively. It thus indicates that both Mn^{2+} and Eu^{2+} enter into the lattice of γ-AlON rather than that of the impurity phase. To further confirm it additional characterization techniques, such as CL and EDS, were attempted.

Cathodoluminescence Spectra and Mapping. In contrast to PL where one incident photon generates one electron−hole pair and only excites levels with lower energies than the incident photon, CL has an incident electron of energy enough to excite the electrons directly into the conduction band. Thus, PL excites just a few emission centers, whereas CL excites all of them. In other words, the CL measurement will help to detect the emissions that cannot be appreciably found or cannot be sure in the PL measurement. As presented in Figure 4a, the CL spectrum of γ-AlON:Eu^{2+},Mn^{2+} (Eu^{2+} = 2 mol %, Mn^{2+} = 5 mol %) is in a good agreement with the PL result (see Figure 2c), indicating that there are no other emission centers than Mn^{2+} and Eu^{2+}. One can see from Figure 4b−d that all of the phosphor particles show both 470 and 517 nm emissions simultaneously, evidencing that both the blue and the green emissions originate from the same γ-AlON lattice.

The cross-sectional CL observation was also performed to confirm the localized luminescence of the γ-AlON:Eu^{2+},Mn^{2+} phosphor. This information can be used to detect if there are any impurity phases inside one phosphor particle. As seen in Figure 5, there is no difference between the 517 and the 470 nm CL images, indicative of the absence of any impurity phase in a luminescent particle, and both of the emissions at 470 and 517 nm stemming from the same host lattice. The elemental distribution of the cross-sectional γ-AlON:Eu^{2+},Mn^{2+} particles was also mapped, as illustrated in Figure 6. Elements of Al, N, O, Mg, Mn, and Eu were uniformly distributed on the same particle, implying that both Eu^{2+} and Mn^{2+} are accommodated in the γ-AlON lattice.

Energy-Transfer Mechanism. A great spectral overlap between the emission band of γ-AlON:Eu^{2+} and the absorption band of γ-AlON:Mn^{2+} is seen in Figure 7. According to the Dexter theory, the mechanism of energy transfer basically requires a spectral overlap between the donor emission band and the acceptor excitation band. Therefore, the energy transfer between the sensitizer (Eu^{2+}) and the activator (Mn^{2+}) in γ-AlON can be speculated.

To further confirm the energy transfer between Eu^{2+} and Mn^{2+} in γ-AlON, the decay time of the emission caused by the

DOI: 10.1021/acs.inorgchem.5b00683
Inorg. Chem. 2015, 54, 5556−5565

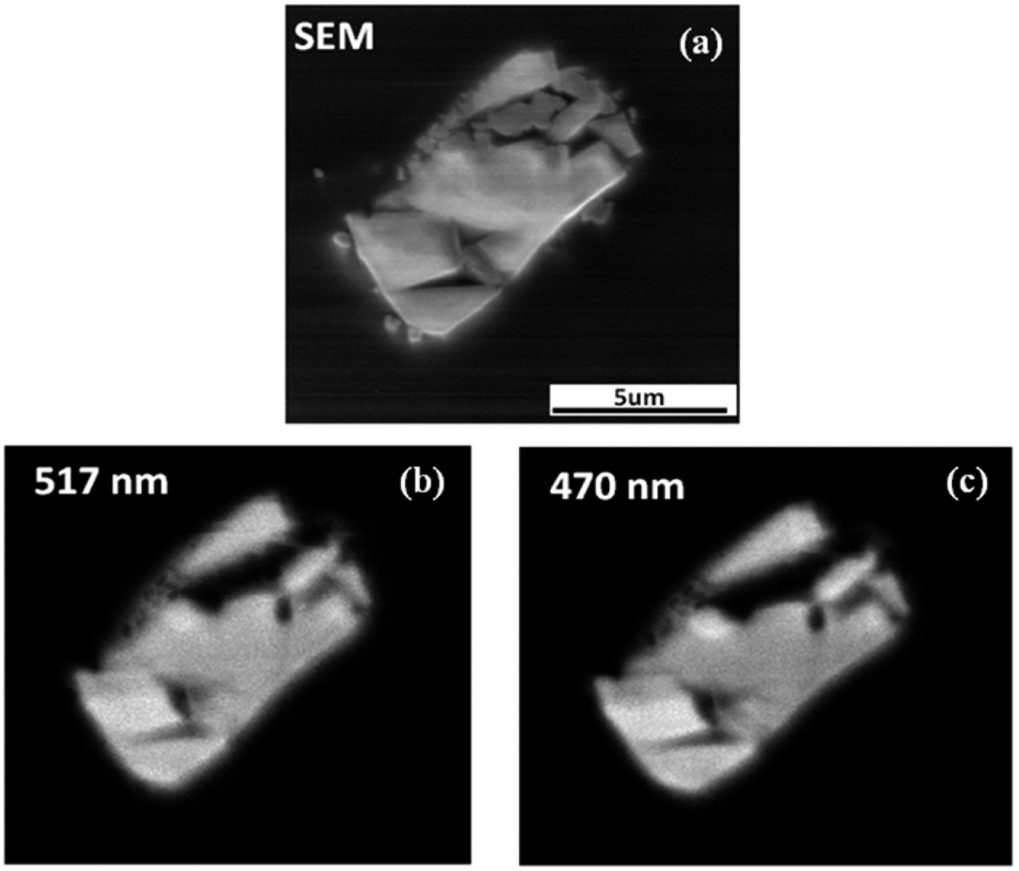

Figure 5. Cross-sectional SEM image (a) and CL images taken at (b) 517 and (c) 470 nm.

energy transfer was measured and fitted using the following equation[29]

$$I = A \exp\left(\frac{-t}{\tau}\right) \quad (1)$$

where I and A are the luminescence intensity at time t and 0, and τ is the luminescence lifetime. The decay curve and decay time of the 470 nm emission of Eu^{2+} in γ-AlON:Eu^{2+},Mn^{2+} phosphors with varying Mn^{2+} concentrations are presented in Figure 8a and 8b. It can be seen that the lifetime of Eu^{2+} reduces from 348 to 145 ns with the increase of the Mn^{2+} amount. The decreased luminescence lifetime of Eu^{2+} with increased Mn^{2+} concentration suggests that the energy absorbed by Eu^{2+} transfers to Mn^{2+}.This is the strong evidence for the energy transfer between Eu^{2+} and Mn^{2+}, and the similar phenomenon has also been reported in the literature.[30,31] Furthermore, the energy-transfer efficiency from Eu^{2+} to Mn^{2+} in γ-AlON (η_T) can be computed by using the following equation[32]

$$\eta_T = 1 - \frac{\tau_s}{\tau_{s0}} \quad (2)$$

where τ_{s0} is the decay time of Eu^{2+} in the absence of Mn^{2+} and τ_s is the decay time of Eu^{2+} in the presence of Mn^{2+}. In γ-AlON:Eu^{2+},Mn^{2+}, η_T was calculated and plotted as a function of the Mn^{2+} concentration (Figure 8c). With increasing Mn^{2+} doping amount, the energy transfer between Eu^{2+} and Mn^{2+} is enhanced greatly. The energy-transfer efficiency is about 50% when the Mn^{2+} concentration is 5 mol %. It increases gradually when the concentration of Mn^{2+} is larger than 5 mol %.

The diagram of Figure 9 presents the luminescence mechanism in γ-AlON:Eu^{2+},Mn^{2+} phosphors. The blue emission of Eu^{2+} originates from electronic transitions of $4f^7-4f^65d$. The energy transfer from Eu^{2+} to Mn^{2+} is via a nonradiative way and results in the enhancement of emission of green light of Mn^{2+} owing to the electronic transition from the $^4T_1$ level to the $^6A_1$ level.

As seen in Figure 10, the Eu^{2+} emission intensity at 470 nm decreases whereas the Mn^{2+} emission at 517 nm enhances as the Mn^{2+} concentration increases, which intuitively indicates the occurrence of energy transfer between Eu^{2+} and Mn^{2+}. Such a change in spectral shape has also been reported in Eu^{2+}- and Mn^{2+}-codoped silicates[33] and phosphates.[22] The change of the spectral shape with increasing Mn^{2+} concentration results in color-tunable emission (from blue-green to green-yellow) in Mn^{2+}- and Eu^{2+}-codoped γ-AlON.

The maximum of the Mn^{2+} emission intensity is reached at 5−7 mol % Mn^{2+} (Figure 11). The observed saturation of intensity may be caused by the $Mn^{2+}-Mn^{2+}$ internal concentration quenching effect. In many cases, concentration quenching is due to the energy transfer from one activator to another until an energy sink in the lattice is reached.[34] The critical distance for the energy transfer between Eu^{2+} and Mn^{2+} (R_{Eu-Mn}) can be calculated by the following formula proposed by Blasse[35]

$$R_{Eu-Mn} = 2[3V/4\pi x_c N]^{1/3} \quad (3)$$

where N is the number of Z ions in the unit cell, V is the volume of the unit cell, and x_c is the total concentration of Eu^{2+} and Mn^{2+}. In this case, N = 8, V = 510.006 Å^3, and x_c = 0.07.

DOI: 10.1021/acs.inorgchem.5b00683
Inorg. Chem. 2015, 54, 5556−5565

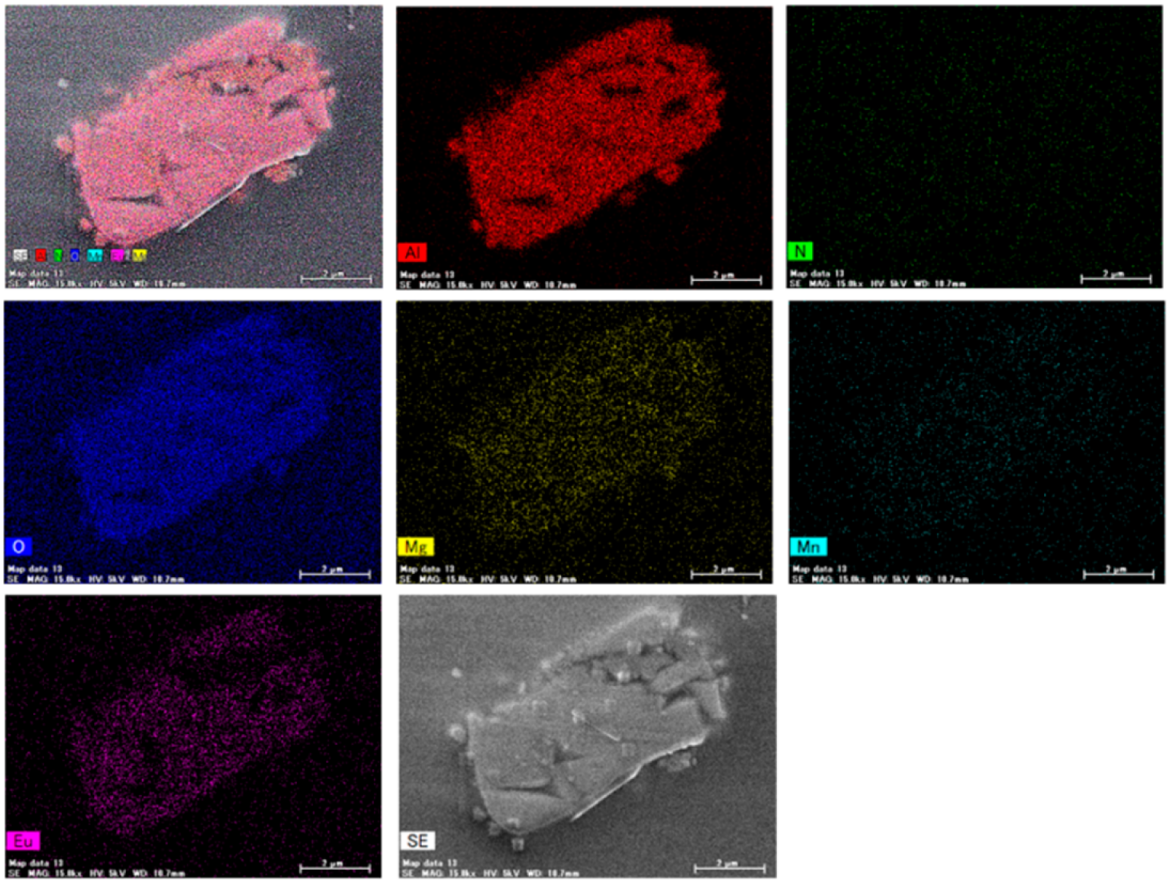

Figure 6. SEM image and elemental mapping of Al, N, O, Mg, Eu, and Mn.

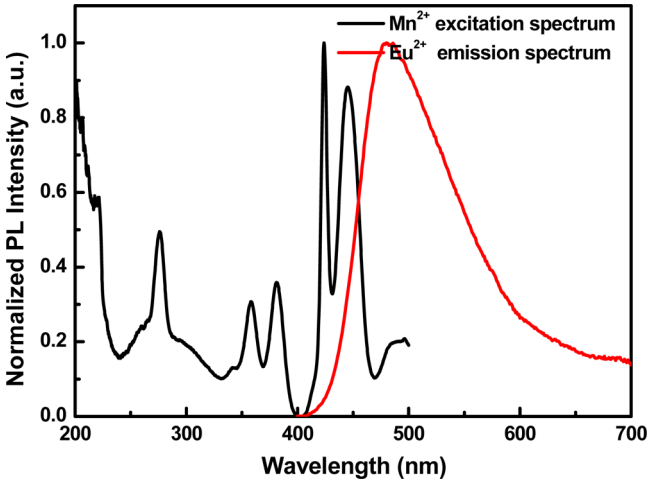

Figure 7. Spectral overlap between the PL excitation spectrum of γ-AlON:Mn^{2+} and the emission spectrum of γ-AlON:Eu^{2+}.

Therefore, the critical distance (R_{Eu-Mn}) for the energy transfer is estimated to be around 12.03 Å. It means that the emission from Eu^{2+} prevails when $R_{Eu-Mn} > R_c$, and the energy transfer from Eu^{2+} to Mn^{2+} dominates when $R_{Eu-Mn} < R_c$. It is well known that if the critical distance between the sensitizer and the activator is shorter than 4 Å, the exchange interaction is responsible for the energy-transfer mechanism. In our case, the R_c value is much bigger than 4 Å, indicating that the energy transfer between Eu^{2+} and Mn^{2+} ions mainly takes place via multipolar interactions. On the basis of Dexter's energy-transfer expressions of multipolar interaction and Reisfeld's approximation, the following relation can be obtained[34]

$$\frac{\eta_0}{\eta} \propto C^{n/3} \tag{4}$$

where η_0 and η are the luminescence quantum efficiency of Eu^{2+} in the absence and presence of Mn^{2+}, C is the sum of the content of Eu^{2+} and Mn^{2+}, and n = 6, 8, and 10 corresponding to dipole−dipole, dipole−quadrupole, and quadrupole−quadrupole interaction, respectively. The value η_0/η can be approximately calculated by the ratio of related luminescence intensity[36,37]

$$\frac{I_{s0}}{I_s} \propto C^{n/3} \tag{5}$$

where I_{s0} is the intrinsic luminescence intensity of Eu^{2+} and I_s is the luminescence of Eu^{2+} in the presence of te Mn^{2+}. The dependence of I_{s0}/I_s of Eu^{2+} on $C^{n/3}$ (n = 6, 8, 10) is plotted in Figure 12. The linear relationship of I_{s0}/I_s versus $C^{n/3}$ is well fitted at n = 6, which clearly indicates that the energy-transfer mechanism is a dipole−dipole interaction type. In this case, the critical distance for the energy transfer can be calculated by the spectral overlap method. Hence, R_c can be achieved from the following formula[38,39]

$$R_c^6 = 3.024 \times 10^{12} \lambda_s^2 f_q \int \frac{F_S(E) F_A(E) dE}{E^4}$$

where f_q (= 10^{-10}) is the oscillator strength of the involved absorption transition of the acceptor (Mn^{2+}), λ_s is the

DOI: 10.1021/acs.inorgchem.5b00683
Inorg. Chem. 2015, 54, 5556−5565

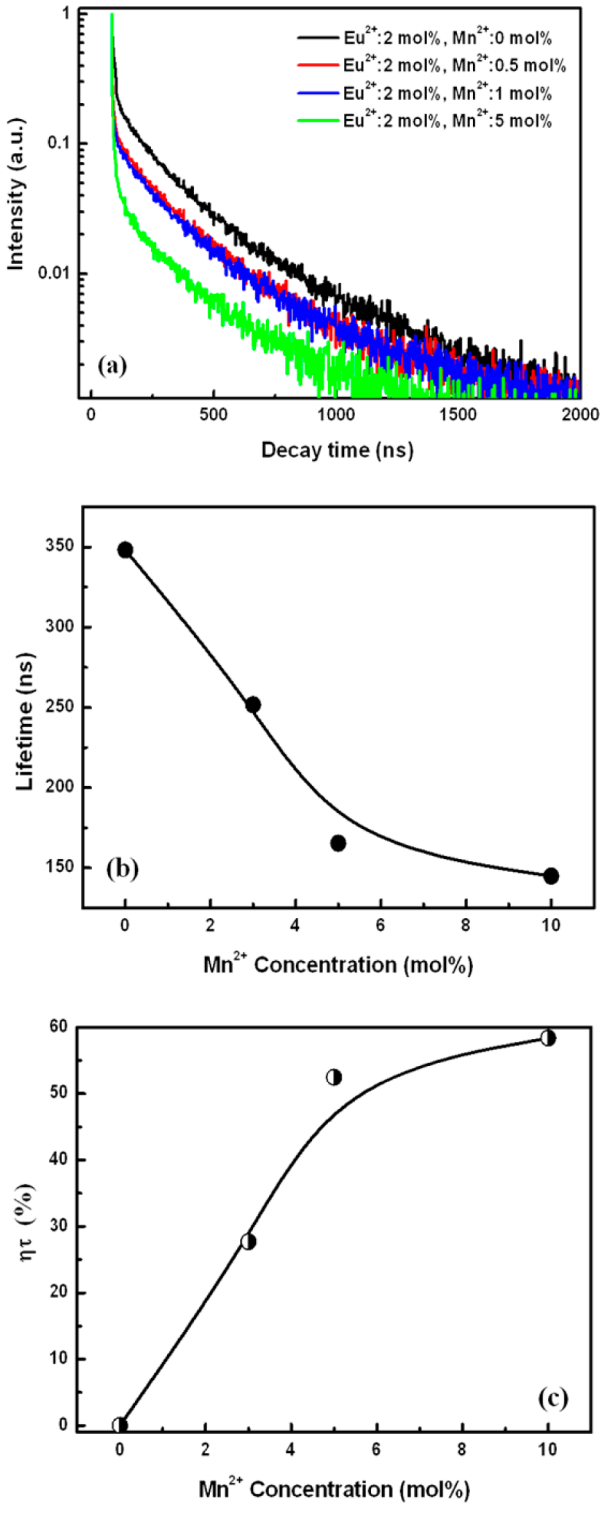

Figure 8. (a) PL decay curves, (b) decay times, and (c) energy-transfer efficiency of γ-AlON:2 mol % Eu^{2+},xMn^{2+} with various amounts of Mn^{2+}.

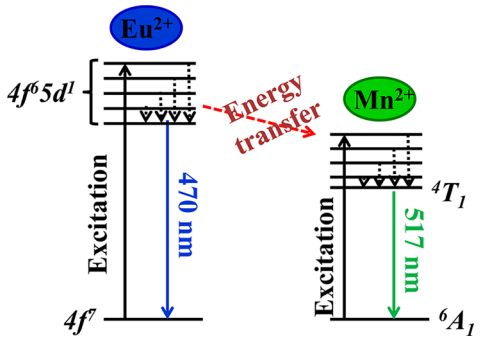

Figure 9. Energy diagram of Eu^{2+} and Mn^{2+} in γ-AlON.

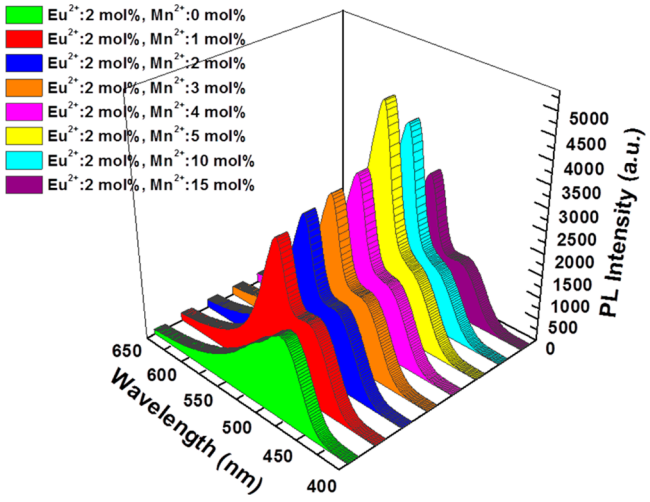

Figure 10. PL spectra of Mn^{2+} in the γ-AlON:Mn^{2+},Eu^{2+} with varying Mn^{2+} concentrations and a fixed Eu^{2+} concentration (2 mol %).

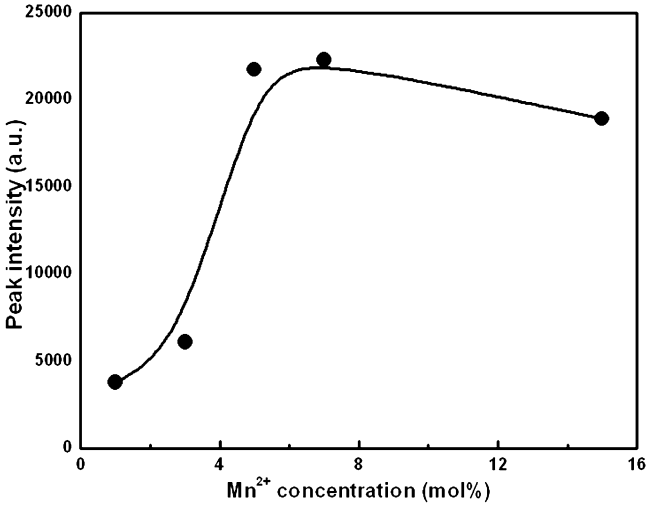

Figure 11. PL intensity of γ-AlON:Mn^{2+},Eu^{2+} (Eu^{2+} = 2 mol %) as a function of Mn^{2+} doping amount.

wavelength position of the sensitizer's emission, E is the energy involved in the transfer, and $\int F_S(E)F_A(E)dE/E^4$ is the spectral overlap between the normalized shapes of the Eu^{2+} emission $F_S(E)$ and the Mn^{2+} excitation $F_A(E)$. In our case, it is calculated to be about 0.0571 eV^{-4}. Using the formula mentioned above, R_c was estimated to be 12.56 Å. This result is in a good agreement with that obtained using the concentration quenching method (12.03 Å), which again confirms the dipole−dipole interaction-induced energy transfer from the Eu^{2+} to Mn^{2+}.

Diffuse Reflectance Spectra. In order to explore the potential of γ-AlON:Mn^{2+},Eu^{2+} to be used as white LEDs phosphors, its photoluminescence properties and thermal quenching were investigated in detail. The diffuse reflection spectra of γ-AlON:Eu^{2+} (Eu^{2+} = 2 mol %), γ-AlON:Mn^{2+}

DOI: 10.1021/acs.inorgchem.5b00683
Inorg. Chem. 2015, 54, 5556−5565

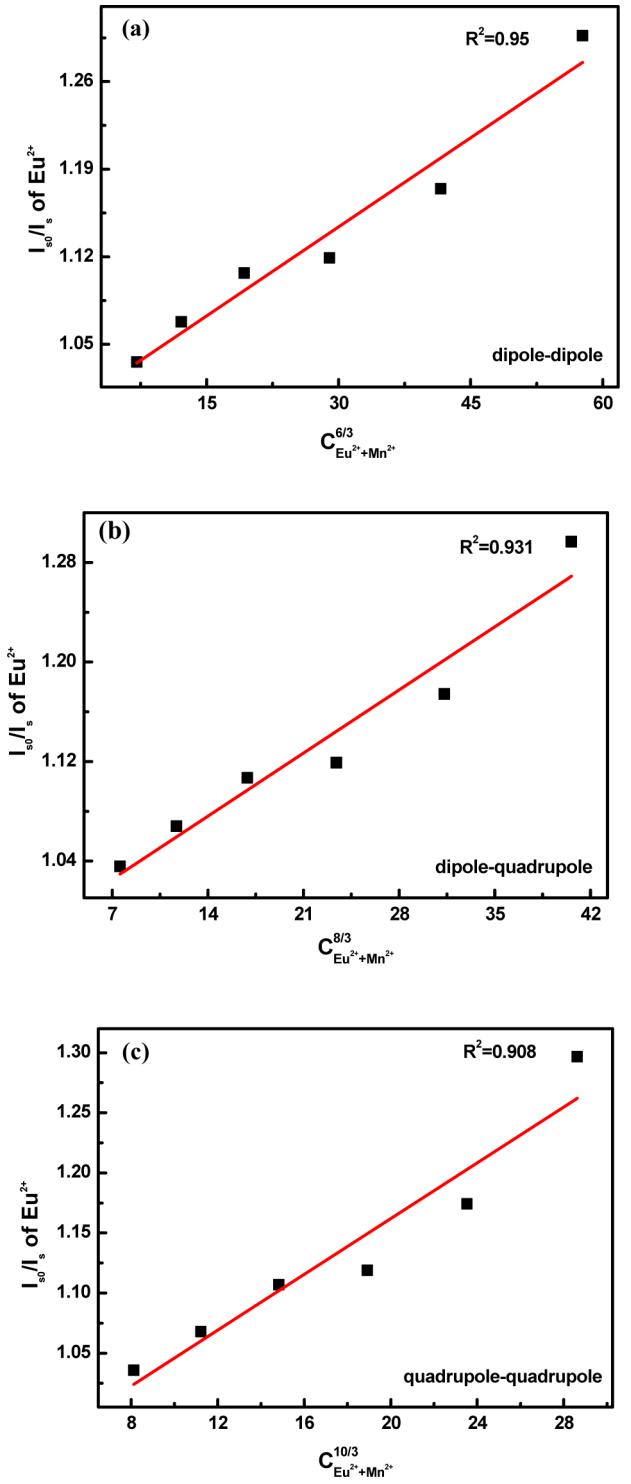

Figure 12. Dependence of I_{s0}/I_s of Eu^{2+} on (a) $C^{6/3}$, (b) $C^{8/3}$, and (c) $C^{10/3}$.

(Mn^{2+} = 5 mol %), and γ-AlON:Mn^{2+},Eu^{2+} (Eu^{2+} = 2 mol %, Mn^{2+} = 5 mol %) are presented in Figure 13. All samples exhibit high reflection at wavelengths of 450−600 nm. The sample singly doped with Eu^{2+} gives strong absorption when the wavelength is below 450 nm. For the sample only doped with Mn^{2+}, it only shows some absorptions at 425 and 446 nm, which are ascribed to the transitions from the ground state of Mn^{2+} to its excited states. In the wavelength range from 300 to 420 nm, however, γ-AlON:Mn^{2+} shows much stronger

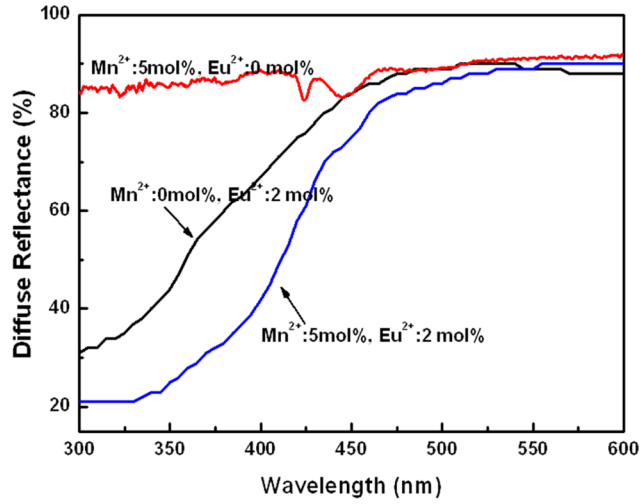

Figure 13. Diffuse reflection spectra of γ-AlON:Eu^{2+} (Eu^{2+} = 2 mol %), γ-AlON:Mn^{2+} (Mn^{2+} = 5 mol %), and γ-AlON:Mn^{2+},Eu^{2+} (Eu^{2+} = 2 mol %, Mn^{2+} = 5 mol %).

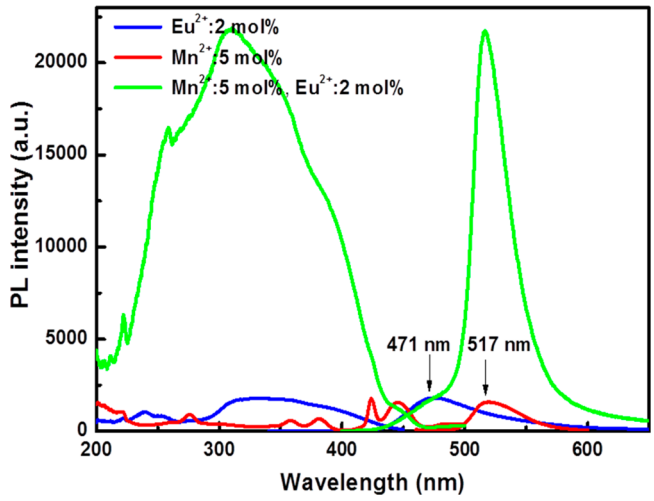

Figure 14. Comparison of PL spectra of γ-AlON:Eu^{2+} (blue), γ-AlON:Mn^{2+} (red), and γ-AlON:Mn^{2+},Eu^{2+} (green).

reflectance than that of γ-AlON:Eu^{2+}, indicative of very weak absorption of UV light for the former sample, while for the sample codoped with Eu^{2+} and Mn^{2+}, the absorption is enhanced strongly at wavelengths shorter than 450 nm, caused by the direct allowed 4f−5d transitions of Eu^{2+} codoped with Mn^{2+} in γ-AlON.

Figure 14 shows the great enhancement at 365 nm for γ-AlON:Mn^{2+},Eu^{2+}, which is consistent with the absorption spectrum shown in Figure 13. The PL intensity of γ-AlON:Mn^{2+},Eu^{2+} at 517 nm is improved by about 9 times with respect to that of γ-AlON:Mn^{2+}, thanks to the strong energy transfer between Eu^{2+} and Mn^{2+}.

As shown in Figure 15, the absorption, internal quantum, and external quantum efficiencies of γ-AlON:Mn^{2+} upon 365 nm excitation are 16%, 48%, and 7%, whereas those of γ-AlON:Mn^{2+},Eu^{2+} are 65%, 75%, and 49%, respectively. The external quantum efficiency is enhanced 7 times by codoping of Eu^{2+}, validating the efficient energy transfer between Eu^{2+} and Mn^{2+}.

Thermal Quenching. The thermal stability of a phosphor has a large impact on the lifetime of wLEDs, so that the

DOI: 10.1021/acs.inorgchem.5b00683
Inorg. Chem. 2015, 54, 5556−5565

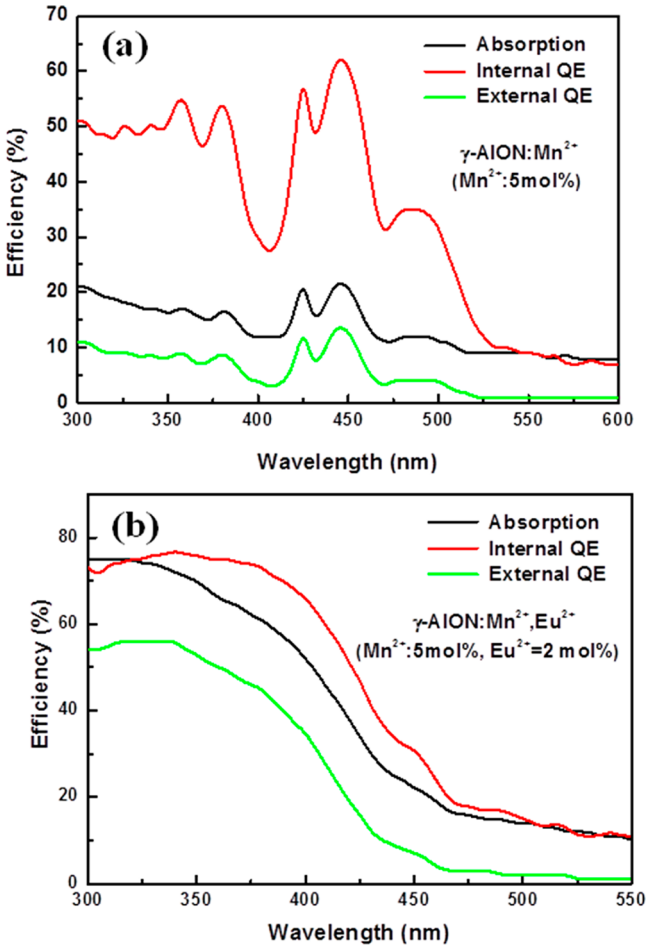

Figure 15. Absorption and quantum efficiencies of (a) γ-AlON:Mn^{2+} (Mn^{2+} = 5 mol %) and (b) γ-AlON:Mn^{2+},Eu^{2+} (Eu^{2+} = 2 mol %, Mn^{2+} = 5 mol %).

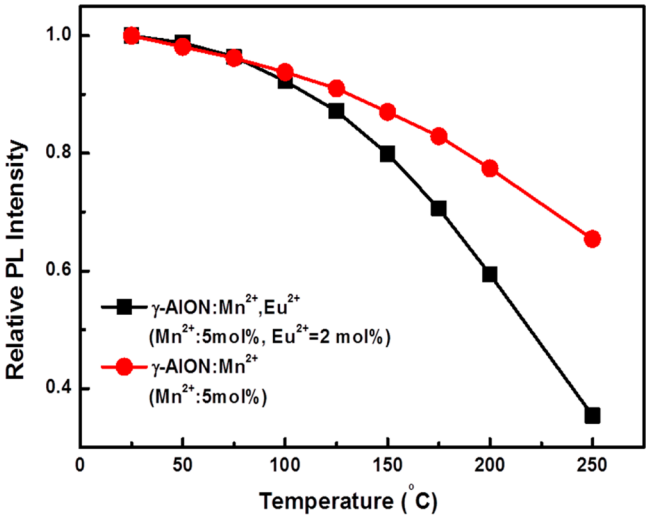

Figure 16. Temperature-dependent luminescence of γ-AlON:Eu^{2+},Mn^{2+} (Eu^{2+} = 2 mol %, Mn^{2+} = 5 mol %) and γ-AlON:Mn^{2+} (Mn^{2+} = 5 mol %). Excitation wavelength is 405 nm.

temperature-dependent luminescence is generally required for understanding the stability of the phosphor against thermal attack. As seen in Figure 16, the emission intensity of γ-ALON:Mn^{2+},Eu^{2+} measured at 150 °C maintains 80% of that measured at room temperature. The thermal quenching is 8% larger than that of γ-ALON:Mn^{2+}[15], but it is still accepted for wLED applications. The larger thermal quenching observed in the codoped sample may be due to the appreciable difference in the ionic radii of Al^{3+} (0.39 Å, 4CN) and Eu^{2+} (1.17 Å, 4CN) than those of Al^{3+} (0.39 Å, 4CN) and Mn^{2+} (0.66 Å, 4CN). When Eu^{2+}−Mn^{2+} were codoped into the γ-AlON lattice, a serious lattice distortion would occur, which enhanced the Stokes shift and finally resulted in a great temperature-dependent luminescence.

This small thermal quenching is ascribed to the excellent thermomechanical properties of γ-AlON with a stiff crystal structure built up on Al−(O,N) tetrahedra and octahedra. The quenching mechanism can be considered as a nonradiative transition. With increasing temperature, the nonradiative transition probability by thermal activation and release of the luminescent center through the crossing point between the excited state and the ground state is enhanced which quenches the luminescence. In this mechanism model, the activation energy (ΔE) for thermal quenching, which is the distance between the excited state of the activator and the crossing point described above, plays a critical role. The activation energy, which is roughly calculated by the Arrhenius equation,[40] is about 0.39 eV for γ-ALON:Mn^{2+},Eu^{2+}. This value is larger than those of α-SiAlON:Yb^{2+} and $Sr_2Si_5N_8$:Eu^{2+} reported in the literature.[41]

CONCLUSIONS

In summary, we synthesized γ-AlON:Eu^{2+},Mn^{2+} phosphors and investigated their luminescence properties and energy-transfer mechanism. The PL and decay time data indicate that the Eu^{2+} → Mn^{2+} energy-transfer process takes place in γ-AlON. The critical energy-transfer distance was calculated by the concentration quenching method and the spectral overlap method. From the experimental results it can be deduced that the mechanism of energy transfer is a resonant type via a dipole−dipole mechanism. Furthermore, we also demonstrated that the PL intensity and absorption and quantum efficiencies of γ-AlON:Eu^{2+},Mn^{2+} measured at 365 nm have been strongly enhanced by the energy transfer between Eu^{2+} and Mn^{2+} in γ-AlON. The PL intensity of γ-AlON:Mn^{2+},Eu^{2+} at 517 nm is improved about 9 times with respect to that of γ-AlON:Mn^{2+}; on the other hand, the external quantum efficiency is enhanced 7 times by codoping of Eu^{2+}. The experimental results show that this kind of phosphor exhibits a potential application for UV white LEDs.

AUTHOR INFORMATION

Corresponding Authors

*Phone: +86-571-86875686. E-mail: calla@cjlu.edu.cn.
*Phone: +81-29-860-4312. Fax: +81-29-851-3613. E-mail: XIE.Rong-Jun@nims.go.jp.

Notes

The authors declare no competing financial interest.

ACKNOWLEDGMENTS

This work was supported in part by Grants-in-Aid for Scientific Research from KAKENHI (Nos. 208551 and 15k06448), National Natural Science Foundation of China (Nos. 51102252, 61177050, and 51272259) and Public Technique Foundation of Zhejiang Province.

DOI: 10.1021/acs.inorgchem.5b00683
Inorg. Chem. 2015, 54, 5556−5565

REFERENCES

(1) Xie, R.-J.; Hirosaki, N. *Sci. Technol. Adv. Mater.* **2007**, *8*, 588−600.
(2) Lin, C. C.; Liu, R. S. *J. Phys. Chem. Lett.* **2011**, *2*, 1268−1277.
(3) Ye, S.; Xiao, F.; Pan, Y. X.; Ma, Y. Y.; Zhang, Q. Y. *Mater. Sci. Eng., R.* **2010**, *71*, 1−34.
(4) Pust, P. A.; Wochnik, S.; Baumann, E.; Schmidt, P. J.; Wiechert, D.; Scheu; Schnick, C. W. *Chem. Mater.* **2014**, *26*, 3544−3549.
(5) Pust, P.; Weiler, V.; Hecht, C.; Tucks, A.; SWochnik, A.; KHenss, A.; Wiechert, D.; Cheu, C. S.; Schmidt, P. J.; Schnick, W. *Nat. Mater.* **2014**, *13*, 891−896.
(6) Hirosaki, N.; Takeda, T.; Funahashi, S.; Xie, R.-J. *Chem. Mater.* **2014**, *26*, 4280−4288.
(7) Schmiechen, S.; Schneider, H.; Wagatha, P.; Hecht, C.; Schmidt, P. J.; Schnick, W. *Chem. Mater.* **2014**, *26*, 2712−2719.
(8) Park, W. B.; Singh, S. P.; Yoon, C.; Sohn, K. S. *J. Mater. Chem.* **2012**, *22*, 14068−14075.
(9) Xie, R.-J.; Hirosaki, N.; Sakuma, K.; Yamamoto, Y.; Mitomo, M. *Appl. Phys. Lett.* **2004**, *84*, 5404−5406.
(10) Li, Y. Q.; van Steen, J. E. J.; van Krevel, J. W. H.; Botty, G.; Delsing, A. C. A.; DiSalvo, F. J.; de With, G.; Hintzen, H. T. *J. Alloys Compd.* **2006**, *417*, 273−279.
(11) Uheda, K.; Hirosaki, N.; Yamamoto, Y.; Naito, A.; Nakajima, T.; Yamamoto, H. *Electrochem. Solid-State Lett.* **2006**, *9*, H22−H25.
(12) Sun, Z. Y. *MRS Bull.* **2009**, *34*, 712−713.
(13) Yin, L. J.; Xu, X.; Hao, L. Y.; Xie, W. J.; Wang, Y. F.; Yang, L. X.; Yang, X. F. *Mater. Lett.* **2009**, *63*, 1511−1513.
(14) Zhang, F.; Chen, S.; Zhang, L. L.; Li, J.; Yang, Y. G.; Zhou, H. H.; Liu, X. J.; Wang, S. W. *J. Am. Ceram. Soc.* **2012**, *95*, 27−29.
(15) Xie, R.-J.; Hirosaki, N.; Liu, X. J.; Takeda, T.; Li, H. L. *Appl. Phys. Lett.* **2008**, *92*, 201905.
(16) Takeda, T.; Xie, R.-J.; Hirosaki, N.; Matsushita, Y.; Honma, T. *J. Solid State Chem.* **2012**, *194*, 71−75.
(17) Sohn, K. S.; Park, E. S.; Kim, C. H.; Park, H. D. *J. Electrochem. Soc.* **2000**, *147*, 4368−4373.
(18) Hao, Z. D.; Nie, Z. G.; Ye, S.; Zhong, R.; Zhang, X. X.; Chen, L.; Ren, X. G.; Lu, S. Z.; Wang, X. J.; Zhang, J. H. *J. Electrochem. Soc.* **2008**, *155*, H606−H610.
(19) Zhou, J.; Wang, Y. H.; Liu, B. T.; Li, F. *J. Appl. Phys.* **2010**, *108*, 033106.
(20) Setlur, A. A.; Shiang, J. J.; Happek, U. *Appl. Phys. Lett.* **2008**, *92*, 081104.
(21) Ma, L.; Wang, D. J.; Mao, Z. Y.; Lu, Q. F.; Yuan, Z. H. *Appl. Phys. Lett.* **2008**, *93*, 144101.
(22) Kwon, K. H.; Bin Im, W.; Jang, H. S.; Yoo, H. S.; Jeon, D. Y. *Inorg. Chem.* **2009**, *48*, 11525−11532.
(23) Chang, C. K.; Chen, T. M. *Appl. Phys. Lett.* **2007**, *90*, 161901.
(24) Shang, M. M.; Li, C. X.; Lin, J. *Chem. Soc. Rev.* **2014**, *43*, 1372−1386.
(25) Li, G. G.; Geng, D. L.; Shang, M. M.; Peng, C.; Cheng, Z. Y.; Lin, J. *J. Mater. Chem.* **2011**, *21*, 13334−13344.
(26) Ding, W. J.; Wang, J.; Liu, Z. M.; Zhang, M.; Su, Q.; Tang, J. K. *J. Electrochem. Soc.* **2008**, *155*, J122−J127.
(27) Yin, L. J.; Yu, W.; Xu, X.; Hao, L. Y. *J. Lumin.* **2012**, *132*, 671−675.
(28) Zhang, F.; Chen, S.; Chen, J. F.; Zhang, H. L.; Li, J.; Liu, X. J.; Wang, S. W. *J. Appl. Phys.* **2012**, *111*, 083532.
(29) Blass, G.; Grabmarier, B. C. *Luminescent Materials*; Springer-Verlag: Berlin, Germany, 1994.
(30) Jiao, H.; Liao, F.; Tian, S.; Jing, X. *J. Electrochem. Soc.* **2003**, *150*, H220−H224.
(31) Ruelle, N.; Pham-Thi, M.; Fouassier, C. *Jpn. J. Appl. Phys.* **1992**, *31*, 2786−2790.
(32) Yang, W. J.; Chen, T. M. *Appl. Phys. Lett.* **2006**, *88*, 101903.
(33) Umetsu, Y.; Okamoto, S.; Yamamoto, H. *J. Electrochem. Soc.* **2008**, *155*, J193−J197.
(34) Dexter, D. L.; Schulman, J. A. *J. Chem. Phys.* **1954**, *22*, 1063−1070.
(35) Blass, G. *Philips Res. Rep.* **1969**, *24*, 131.
(36) Yang, W. J.; Luo, L. Y.; Chen, T. M.; Chen, N. S. *Chem. Mater.* **2005**, *17*, 3883−3888.
(37) Van Uitert, L. G. *J. Electrochem. Soc.* **1967**, *114*, 1048−1053.
(38) Guo, N.; Huang, Y. J.; You, H. P.; Yang, M.; Song, Y. H.; Liu, K.; Zheng, Y. H. *Inorg. Chem.* **2010**, *49*, 10907−10913.
(39) You, H. P.; Zhang, J. L.; Hong, G. Y.; Zhang, H. J. *J. Phys. Chem. C* **2007**, *111*, 10657−10661.
(40) Bhushan, S.; Chukichev, M. V. *J. Mater. Sci. Lett.* **1988**, *7*, 319−321.
(41) Xie, R.-J.; Hirosaki, N.; Kimura, N.; Sakuma, K.; Mitomo, M. *Appl. Phys. Lett.* **2007**, *90*, 191101.

DOI: 10.1021/acs.inorgchem.5b00683
Inorg. Chem. 2015, 54, 5556−5565